Exact Green's function for a multiorbital Anderson impurity at high bias voltages

Akira Oguri[1] and Rui Sakano[2]

[1]*Department of Physics, Osaka City University, Sumiyoshi-ku, Osaka 558-8585, Japan*
[2]*The Institute for Solid State Physics, The University of Tokyo, Kashiwa, Chiba 277-8581, Japan*

We study the nonequilibrium Keldysh Green's function for an N-orbital Anderson model at high bias voltages, extending a previous work which for the case only with the spin degrees of freedom $N = 2$ to arbitrary N. Our approach uses an effective non-Hermitian Hamiltonian that is defined with respect to a Liouville-Fock space in the context of a thermal field theory. The result correctly captures the relaxation processes at high energies, and is asymptotically exact not only in the high bias limit, but also in the high-temperature limit at thermal equilibrium. We also present an explicit continued-fraction representation of the Green's function. It clearly shows that the imaginary part is recursively determined by the decay rate of intermediate states with at most $N - 1$ particle-hole-pair excitations. These high bias properties follow from the conservations of a generalized charge and current in the Liouville-Fock space. We also examine temperature dependence of the spectral function in equilibrium, comparing the exact results with the numerical finite-T and analytical $T \to \infty$ results of the noncrossing approximation.

I. INTRODUCTION

Role of the orbital degrees of freedom has been one of the key issues in quantum dots and dilute magnetic alloys [1,2]. It also gives a variety in the many-body effects, such as the Kondo effect and Coulomb blockade, in a wide energy scale [3–8]. Specifically, the orbital degeneracy affects the nonequilibrium current and current noise of quantum dots driven by the bias voltage eV, and has recently been studied in the low-energy Fermi-liquid regime [9–12].

However, further investigations of higher-energy regions beyond the Fermi-liquid regime are still needed to comprehensively explore the orbital effects on the correlated electrons in quantum dots. There are some efficient numerical approaches that can provide information relevant to the intermediate-energy regions. For instance, the Wilson numerical renormalization group (NRG) [13], the density matrix renormalization group [14], the continuous-time quantum Monte Carlo methods [15,16], and the Matsubara-voltage approach [17] can be applied to the multiorbital Anderson model for quantum dots in the case where the internal degrees of freedom N are not so large. Alternatively, perturbative large-N approaches, such as the noncrossing approximation (NCA) [18–22] and $1/(N-1)$ expansion [23,24], can explore the parameter regions complementary to the numerical ones.

We have previously considered the high bias limit of the $N = 2$ Anderson model [25,26], for which nonequilibrium quantum transport in the low-energy Fermi-liquid region has been investigated for a long time [27–35]. We have shown that the Keldysh Green's function [36,37] is solvable in the opposite limit $eV \to \infty$, where the excitations of whole energy scales equally contribute to the dynamics. In this limit, the model can be mapped onto a non-Hermitian Hamiltonian of two effective sites in a doubled Hilbert space that is defined in the thermal field theory [38,39]. The asymptotically exact Green's function for $eV \to \infty$ has a similar form to the atomic-limit solution of Hubbard I [40–42], but is still nontrivial as the hybridization energy scale Δ ($\equiv \Gamma_L + \Gamma_R$) that competes

with the Coulomb repulsion U is fully taken into account without any assumptions. For this reason, the result correctly captures the imaginary part due to the relaxation processes, which in the high bias limit is determined by the damping of a single-particle accompanied by a virtually excited particle-hole pair in the intermediate states. Furthermore, it has also been clarified that the spectral weight depends sensitively on the asymmetry in Γ_L and Γ_R, which are the hybridizations between the impurity and the reservoirs on the left and right, respectively.

In this paper, we extend the formulation to treat the multiorbital Anderson model, and provide the asymptotically exact high bias Green's function for generic two-body interactions $U_{mm'}$ between the electrons in different orbitals m and m' with orbital-dependent hybridizations $\Gamma_{L,m}$ and $\Gamma_{R,m}$. The thermal-field-theoretical approach [38,39] that we use is equivalent to the Keldysh formalism. However, the time evolution along the backward Keldysh contour is dealt with in a different way, using fictitious fermions defined with respect to the enlarged Hilbert space. It is also referred to as a Liouville-Fock space and has been applied to quantum-transport problems [43–46]. We show that the effective non-Hermitian Hamiltonian can be expressed in terms of a generalized charge and current, which commute each other, also in the multiorbital case. This algebraic structure makes the many-body effects on the Green's function and other dynamic correlation functions separable in the time representation. The exact Green's function can be expressed in a factorized form, which consists of contributions of the intermediate particle-hole-pair excitations from each of the orbitals.

For the m-independent interactions and hybridizations, namely for U, Γ_L, and Γ_R, we also obtain the continued-fraction representation of the Green's function for arbitrary N as a function of frequency ω. The results show that the spectral function has N distinguishable peaks, the height of which is determined by the binominal distribution, specifically for symmetric hybridizations $\Gamma_L = \Gamma_R$ and strong interactions $U \gg \Delta$. In the continued-fraction representation, the

imaginary part due to the relaxation of the intermediate state with $k\ (=1,2,\ldots,N-1)$ particle-hole-pair excitations recursively emerges through the iteration that terminates after $N-1$ steps.

Our results also describe the high-temperature limit at equilibrium $eV=0$, where the Fermi function becomes an ω-independent constant $f(\omega) \to \frac{1}{2}$. We also examine temperature dependence of the spectral function of the particle-hole-symmetric SU(4) Anderson model, using the NCA which can also be analytically solved in the limit of $T \to \infty$. Near the Kondo temperature $T \simeq T_K$, besides the Kondo peak at the Fermi level $\omega=0$, not all the four subpeaks of the atomic nature can be seen yet but the lower two subpeaks can be at $\omega = \pm U/2$. It is at much higher temperatures $T \gg T_K$ that the higher-energy subpeaks emerge at $\omega = \pm 3U/2$. The NCA reasonably describes these features of the temperature dependence although there are some quantitative deviations from the exact results in the high-temperature limit. The analytic solution can also be used in such a way as a standard for comparisons to check the accuracy of any approximations.

This paper is organized as follows. We describe the relation between the Keldysh formalism and the thermal-field-theoretical approach in Sec. II. The effective non-Hermitian Hamiltonian for the high bias limit is introduced in Sec. III. The initial and final states for the time-dependent perturbation theory are introduced with the nonequilibrium density matrix for the Liouville-Fock space in Sec. IV. General properties of the dynamic correlation functions, which can be deduced from the charge and current conservations in the Liouville-Fock space for $eV \to \infty$, are discussed in Sec. V. The derivation of exact high bias Green's function for generic two-body interactions $U_{mm'}$ is given in Sec. VI. The continued fraction representation of the Green's function for the m-independent interaction U and properties of the spectral function are described in Sec. VII. Summary is given in Sec. VIII.

II. KELDYSH FORMALISM

We start with a multiorbital Anderson impurity coupled to two noninteracting leads ($\alpha = L, R$). The Hamiltonian is given by $\mathcal{H} = \mathcal{H}_0 + \mathcal{H}_U$ with

$$\mathcal{H}_0 = \sum_{m=1}^{N} \varepsilon_{d,m}\, n_{d,m} + \sum_{\alpha=L,R}\sum_{m=1}^{N} v_{\alpha,m} (d_m^\dagger \psi_{\alpha m} + \text{H.c.})$$

$$+ \sum_{\alpha=L,R}\sum_{m=1}^{N} \int_{-D}^{D} d\epsilon\, \epsilon\, c_{\epsilon\alpha m}^\dagger c_{\epsilon\alpha m}, \qquad (1)$$

$$\mathcal{H}_U = \frac{1}{2}\sum_{m\neq m'} U_{mm'}\, n_{d,m} n_{d,m'}. \qquad (2)$$

Here, $n_{d,m} = d_m^\dagger d_m$ describes the local charge in the quantum dot, and $d_m^\dagger$ creates an electron in a one-particle state with a quantum number $m\ (=1,2,\ldots,N)$ whose eigenenergy $\varepsilon_{d,m}$ generally depends on m, for instance, in a finite magnetic field. The interelectron interaction $U_{mm'}$ generally depends on m and m', with a requirement $U_{mm'} = U_{m'm}$. The operator $c_{\epsilon\alpha m}^\dagger$ creates a conduction electron with energy ϵ in orbital m for the lead on the left $\alpha = L$ or right $\alpha = R$. It is normalized such that

$\{c_{\epsilon\alpha m}, c_{\epsilon'\alpha'm'}^\dagger\} = \delta_{\alpha\alpha'}\, \delta_{mm'}\delta(\epsilon-\epsilon')$. The linear combination of the conduction electrons, defined by $\psi_{\alpha m} \equiv \int_{-D}^{D} d\epsilon \sqrt{\rho_c}\, c_{\epsilon\alpha m}$ with $\rho_c = 1/(2D)$, couples to the quantized levels of the dot via the hybridization matrix element $v_{\alpha,m}$. This hybridization causes an m-dependent level broadening of the energy scale $\Delta_m \equiv \Gamma_{L,m} + \Gamma_{R,m}$ with $\Gamma_{\alpha,m} = \pi \rho_c\, v_{\alpha,m}^2$. We consider the parameter region where the half-bandwidth D is much greater than the other energy scales $D \gg \max(U_{mm'}, \Delta_m, |\varepsilon_{d,m}|, T, eV)$ unless otherwise noted.

Nonequilibrium steady state under a finite bias voltage can be described by the Keldysh formalism [27,28,36,37]. Specifically, we use an effective action $\mathcal{S} = \mathcal{S}_0 + \mathcal{S}_U$ that determines the time evolution along the Keldysh contour

$$\mathcal{Z} = \int D\bar{\eta}\, D\eta\; e^{i\,[\,\mathcal{S}_0(\bar{\eta},\eta) + \mathcal{S}_U(\bar{\eta},\eta)\,]}, \qquad (3)$$

$$\mathcal{S}_0 = \sum_{m=1}^{N} \int_{-\infty}^{\infty} dt\, dt'\; \overline{\boldsymbol{\eta}}_m(t)\, \boldsymbol{K}_{0,m}(t,t')\, \boldsymbol{\eta}_m(t'), \qquad (4)$$

$$\mathcal{S}_U = -\frac{1}{2}\sum_{m\neq m'} U_{mm'} \int_{-\infty}^{\infty} dt$$

$$\times\,\{\,\overline{\eta}_{-,m}(t)\,\eta_{-,m}(t)\,\overline{\eta}_{-,m'}(t)\,\eta_{-,m'}(t)$$

$$-\,\overline{\eta}_{+,m}(t)\,\eta_{+,m}(t)\,\overline{\eta}_{+,m'}(t)\,\eta_{+,m'}(t)\}. \qquad (5)$$

Here, $\overline{\boldsymbol{\eta}}_m = (\overline{\eta}_{-,m}, \overline{\eta}_{+,m})$ is a pair of the Grassmann numbers for the $-$ and $+$ branches of the Keldysh contour. The kernel $\boldsymbol{K}_{0,m}(t,t')$ is given by the Fourier transform of the noninteracting Green's function

$$\boldsymbol{K}_{0,m}(t,t') = \int_{-\infty}^{\infty} \frac{d\omega}{2\pi}\, \{\boldsymbol{G}_{0,m}(\omega)\}^{-1} e^{-i\omega(t-t')}, \qquad (6)$$

$$\{\boldsymbol{G}_{0,m}(\omega)\}^{-1} = (\omega - \varepsilon_{d,m})\, \boldsymbol{\tau}_3 - \boldsymbol{\Sigma}_{0,m}(\omega), \qquad (7)$$

$$\boldsymbol{\Sigma}_{0,m}(\omega) = -i\Delta_m\big[\,1 - 2 f_{\text{eff}}^{(m)}(\omega)\,\big](\boldsymbol{1} - \boldsymbol{\tau}_1) + \Delta_m \boldsymbol{\tau}_2. \qquad (8)$$

Here, $\boldsymbol{1}$ is the 2×2 unit matrix and $\boldsymbol{\tau}_j$ for $j = 1,2,3$ are the Pauli matrices,

$$\boldsymbol{\tau}_1 = \begin{pmatrix} 0 & 1 \\ 1 & 0 \end{pmatrix}, \quad \boldsymbol{\tau}_2 = \begin{pmatrix} 0 & -i \\ i & 0 \end{pmatrix}, \quad \boldsymbol{\tau}_3 = \begin{pmatrix} 1 & 0 \\ 0 & -1 \end{pmatrix}. \qquad (9)$$

The distribution function $f_{\text{eff}}^{(m)}(\omega)$ is defined by

$$f_{\text{eff}}^{(m)}(\omega) = \frac{\Gamma_{L,m}\, f_L(\omega) + \Gamma_{R,m}\, f_R(\omega)}{\Gamma_{L,m} + \Gamma_{R,m}}, \qquad (10)$$

where $f_\alpha(\omega) = [\,e^{(\omega - \mu_\alpha)/T} + 1\,]^{-1}$ and μ_α is the chemical potential for lead α. This distribution function describes the energy window as depicted in Fig. 1, and determines the long-time behavior of $\boldsymbol{K}_{0,m}(t,t')$ as a function of $t - t'$. Furthermore, temperature T and bias voltage $eV \equiv \mu_L - \mu_R$ enter through $f_{\text{eff}}^{(m)}(\omega)$ for impurity correlation functions.

III. LIOUVILLE-FOCK SPACE FOR $eV \to \infty$

We consider two kinds of the high-energy limits in this work. One is the high bias limit $eV \gg T$, where $f_L \to 1$
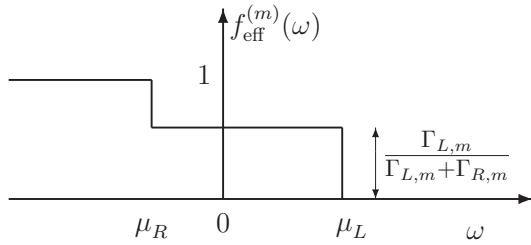
FIG. 1. The nonequilibrium distribution function $f_{\text{eff}}^{(m)}(\omega)$ for $\mu_L - \mu_R = eV$ and $T = 0$. The Fermi level at equilibrium $eV = 0$ is chosen to be the origin of energy $\omega = 0$.

and $f_R \to 0$. The other is high-temperature limit $T \gg eV$ where $f_L = f_R \to \frac{1}{2}$, and this includes thermal equilibrium at $eV = 0$ as a special case. In both of these two limits, the distribution function $f_{\text{eff}}^{(m)}(\omega)$ becomes a constant independent of the frequency ω:

$$f_{\text{eff}}^{(m)}(\omega) \to \begin{cases} \frac{\Gamma_{L,m}}{\Gamma_{L,m} + \Gamma_{R,m}} & \text{for} \quad eV \to \infty, \\ \frac{1}{2} & \text{for} \quad T \to \infty. \end{cases} \quad (11)$$

Then, the hybridization self-energy $\boldsymbol{\Sigma}_{0,m}(\omega)$ also becomes independent of ω, and then excitations of whole energy scales equally contribute to the dynamics. This makes the problems in the high-energy limits solvable. In the following, we concentrate on the $eV \to \infty$ limit because the $T \to \infty$ limit is equivalent to the symmetric coupling case $\Gamma_{L,m} = \Gamma_{R,m}$ of the high bias limit as long as local properties near the impurity site are concerned.

A. Effective non-Hermitian Hamiltonian

In the high bias limit, the hybridization self-energy defined in Eq. (8) is given by an ω-independent matrix

$$\lim_{eV \to \infty} \boldsymbol{\Sigma}_{0,m}(\omega) = \boldsymbol{\tau}_3 \, \boldsymbol{L}_{0,m}, \quad (12)$$

$$\boldsymbol{L}_{0,m} \equiv i \begin{bmatrix} \Gamma_{L,m} - \Gamma_{R,m} & -2\Gamma_{L,m} \\ -2\Gamma_{R,m} & -(\Gamma_{L,m} - \Gamma_{R,m}) \end{bmatrix}. \quad (13)$$

Then, the kernel $\boldsymbol{K}_{0,m}(t,t')$ takes a Markovian form with a linear combination of $\delta(t - t')$ and its derivative. The derivative arises from the ω linear part of $\{\boldsymbol{G}_{0,m}(\omega)\}^{-1}$, and the noninteracting part of the action $\mathcal{S}_0$ can be expressed in a single integration with respect to t:

$$\mathcal{S}_0 \to \sum_{m=1}^{N} \int_{-\infty}^{\infty} dt \, \boldsymbol{\eta}_m^{\dagger}(t) \left\{ \mathbf{1}\left(i\frac{\partial}{\partial t} - \varepsilon_{d,m}\right) - \boldsymbol{L}_{0,m} \right\} \boldsymbol{\eta}_m(t). \quad (14)$$

Here, the transformation $\boldsymbol{\eta}_m^{\dagger} = \overline{\boldsymbol{\eta}}_m \, \boldsymbol{\tau}_3$ has been introduced only for the conjugate part of the Grassmann numbers, keeping the counter part $\boldsymbol{\eta}_m$ unchanged. This transform makes the time-derivative term $\mathcal{S}_0$ diagonal, keeping the interacting action $\mathcal{S}_U$ in a similar form:

$$\mathcal{S}_U = -\frac{1}{2} \sum_{m \neq m'} U_{mm'} \int_{-\infty}^{\infty} dt \, \{\eta_{-,m}^{\dagger}(t) \, \eta_{-,m}(t) \, \eta_{-,m'}^{\dagger}(t) \, \eta_{-,m'}(t)$$
$$- \eta_{+,m}^{\dagger}(t) \, \eta_{+,m}(t) \, \eta_{+,m'}^{\dagger}(t) \, \eta_{+,m'}(t)\}. \quad (15)$$

Therefore, in the high bias limit, the Lagrangian that corresponds to the integrand of $\mathcal{S}_0 + \mathcal{S}_U$ does not have an explicit time dependence other than the first derivative $i\partial/\partial t$ term in Eq. (14). The contributions of the conduction electrons enter through $\boldsymbol{L}_{0,m}$. The Lagrangian of this form can also be constructed from a non-Hermitian Hamiltonian defined with respect to the doubled Hilbert space, consisting only of the impurity degrees of freedom: $\widehat{H}_{\text{eff}} = \widehat{H}_{\text{eff}}^{(0)} + \widehat{H}_{\text{eff}}^{(U)}$,

$$\widehat{H}_{\text{eff}}^{(0)} \equiv \sum_{m=1}^{N} \xi_{d,m}(n_{-,m} + n_{+,m} - 1)$$
$$+ \sum_{m=1}^{N} (\boldsymbol{d}_m^{\dagger} \boldsymbol{L}_{0,m} \boldsymbol{d}_m - i \Delta_m), \quad (16)$$

$$\widehat{H}_{\text{eff}}^{(U)} \equiv \frac{1}{2} \sum_{m \neq m'} U_{mm'} \left[\left(n_{-,m} - \frac{1}{2}\right)\left(n_{-,m'} - \frac{1}{2}\right) \right.$$
$$\left. - \left(n_{+,m} - \frac{1}{2}\right)\left(n_{+,m'} - \frac{1}{2}\right) \right]. \quad (17)$$

Here,

$$\xi_{d,m} = \varepsilon_{d,m} + \frac{1}{2} \sum_{m'(\neq m)} U_{mm'}, \quad (18)$$

and $\boldsymbol{d}_m^{\dagger} = (d_{-,m}^{\dagger}, d_{+,m}^{\dagger})$ is a set of two independent fermion operators introduced for the $-$ and $+$ branches, respectively, and $n_{\mu,m} = d_{\mu,m}^{\dagger} d_{\mu,m}$. In this representation, the fermion operators with the label "$-$" describe the original impurity electron $d_{-,m}^{\dagger} \equiv d_m^{\dagger}$. The other component with the label "$+$" corresponds to a tilde-conjugate operator $\widetilde{d}_m^{\dagger}$ in the standard notation of the thermal field theory [38,39]. Specifically, our representation uses a particle-hole transformed version where $d_{+,m}^{\dagger} \equiv \widetilde{d}_m$.

Note that the conduction degrees of freedom have been effectively decoupled, and the extended Hilbert space for the impurity states, which is referred to as Liouville-Fock space [43–46] in the following, consists of 2^{2N} basis sets. The time evolution of the state vectors in this space is described by the Heisenberg operators [38,39]

$$\mathcal{O}(t) \equiv e^{i\widehat{H}_{\text{eff}} t} \mathcal{O} \, e^{-i\widehat{H}_{\text{eff}} t}, \quad (19)$$

$$i \frac{\partial \mathcal{O}(t)}{\partial t} = [\mathcal{O}(t), \widehat{H}_{\text{eff}}]. \quad (20)$$

B. Charge and current representation

One of the merits of the effective Hamiltonian formulation is that it can clearly extract the properties that system acquires in the high bias limit. In order to see the precise features, we rewrite the interaction part defined in Eq. (17) in the form

$$\widehat{H}_{\text{eff}}^{(U)} = \frac{1}{2} \sum_{m \neq m'} U_{mm'} (Q_m q_{m'} + Q_{m'} q_m)$$
$$= \sum_{m=1}^{N} q_m \widehat{(UQ)}_m. \quad (21)$$

Here, the operators Q_m, q_m, and $\widehat{(UQ)}_m$ are defined by

$$Q_m \equiv n_{-,m} + n_{+,m} - 1, \qquad q_m \equiv \frac{n_{-,m} - n_{+,m}}{2}, \quad (22)$$

$$\widehat{(UQ)}_m \equiv \sum_{m'(\neq m)} U_{mm'} Q_{m'}. \quad (23)$$

The operator $\widehat{(UQ)}_m$ corresponds to the potential that is induced in the orbital m by the particles occupying the other orbitals $m'(\neq m)$. Note that this potential $\widehat{(UQ)}_m$ vanishes identically in the subspace where $Q_{m'} = 0$ for all m' (= $1, 2, \ldots, N$). This happens for the final and initial states $\langle\!\langle I\|$ and $\|\rho\rangle\!\rangle$, which are introduced in the next section for the time-dependent perturbation theory in the Liouville-Fock space.

The off-diagonal components of $\widehat{H}_{\text{eff}}$ can be regarded as the operators, equivalent to the current $I_{R,m}$ flowing from the dot to the right lead and $I_{L,m}$ flowing from the left lead to the dot,

$$I_{R,m} = -2\Gamma_{R,m} d_{+,m}^{\dagger} d_{-,m}, \quad I_{L,m} = -2\Gamma_{L,m} d_{-,m}^{\dagger} d_{+,m}. \quad (24)$$

Although these are non-Hermitian, the operator equivalence holds with respect to the Liouville-Fock space. Using these charge and current operators, the effective Hamiltonian can be expressed in the form

$$\widehat{H}_{\text{eff}} = \sum_{m=1}^{N} \xi_{d,m} Q_m + i \sum_{m=1}^{N} (P_m - \Delta_m), \quad (25)$$

$$P_m \equiv I_{R,m} + I_{L,m} + 2\mathcal{W}_m q_m, \quad (26)$$

$$\mathcal{W}_m \equiv (\Gamma_{L,m} - \Gamma_{R,m}) - i\frac{1}{2}\widehat{(UQ)}_m. \quad (27)$$

The two operators Q_m and P_m commute each other, and also commute, respectively, with $\widehat{H}_{\text{eff}}$:

$$[Q_m, P_{m'}] = 0, \quad [Q_m, \widehat{H}_{\text{eff}}] = 0, \quad [P_m, \widehat{H}_{\text{eff}}] = 0. \quad (28)$$

Therefore, Q_m and P_m are conserved, and $\widehat{H}_{\text{eff}}$ acquires a highly symmetrical algebraic structure. The equations of motion for the relative charge q_m and the relative current p_m constitute a closed system

$$\frac{\partial q_m}{\partial t} = -p_m, \quad p_m \equiv I_{R,m} - I_{L,m}, \quad (29)$$

$$\frac{\partial p_m}{\partial t} = 4\mathcal{L}_m^2 q_m + 2\mathcal{W}_m P_m, \quad (30)$$

$$\mathcal{L}_m^2 \equiv \frac{1}{4}\{\widehat{(UQ)}_m\}^2 + i(\Gamma_{L,m} - \Gamma_{R,m})\widehat{(UQ)}_m - \Delta_m^2. \quad (31)$$

It is also deduced from Eqs. (28)–(30) that the second derivative of p_m satisfies the equation

$$\frac{\partial^2 p_m}{\partial t^2} = -4\mathcal{L}_m^2 p_m. \quad (32)$$

The operator $\mathcal{L}_m^2$ plays a central role on the relaxation phenomena in the high bias limit. Specifically, in the subspace where $\widehat{(UQ)}_m = 0$, the eigenvalue of $\mathcal{L}_m^2$ is given simply

by $-\Delta_m^2$, and the Heisenberg operators of p_m and q_m can be expressed as a linear combination of $e^{2\Delta_m t}$ and $e^{-2\Delta_m t}$. Here, the relaxation rate $2\Delta_m$ is determined by a damping of a particle-hole-pair excitation [26]. Furthermore, it can be deduced from these properties that in the high bias limit, a wide class of the susceptibilities of the charges and currents become identical to those for the noninteracting electrons as shown in Sec. V A.

IV. INTERACTION REPRESENTATION FOR THE NON-HERMITIAN HAMILTONIAN

We have introduced in the above $\widehat{H}_{\text{eff}}$ corresponds to the effective action $\mathcal{S}_0 + \mathcal{S}_U$. In order to complete the full description, we need to specify the density matrix that determines the nonequilibrium distribution. Furthermore, it is also necessary to impose some conditions as the fermion operators $d_{+,m}$ of the $+$ branch describe the same physical particle as that of the $-$ branch at the turnaround point $t \to \infty$ of the Keldysh contour. As we see in the following, the time-dependent perturbation theory for the Liouville-Fock space can be constructed in a way such that these requirements can be fulfilled through the properly chosen final $\langle\!\langle I\|$ and initial $\|\rho\rangle\!\rangle$ states [47].

To this end, we consider the time evolution in more detail in the interaction representation

$$\widehat{\mathcal{U}}(t_2, t_1) \equiv \text{T} \exp\left[-i\int_{t_1}^{t_2} dt\, e^{i\widehat{H}_{\text{eff}}^{(0)}t}\widehat{H}_{\text{eff}}^{(U)}e^{-i\widehat{H}_{\text{eff}}^{(0)}t}\right], \quad (33)$$

$$\mathcal{O}^{\mathcal{I}}(t) \equiv e^{i\widehat{H}_{\text{eff}}^{(0)}t}\,\mathcal{O}\,e^{-i\widehat{H}_{\text{eff}}^{(0)}t}, \quad (34)$$

where T is the usual time-ordering operator along the branch of $-\infty < t < \infty$.

A. Final and initial states: $\langle\!\langle I\|$ and $\|\rho\rangle\!\rangle$

The free part of the effective Hamiltonian can be rewritten in a diagonal form

$$\widehat{H}_{\text{eff}}^{(0)} = \sum_m \xi_{d,m}\left(a_m^{-1}a_m + b_m^{-1}b_m - 1\right)$$
$$+ \sum_m i\Delta_m\left(a_m^{-1}a_m - b_m^{-1}b_m - 1\right). \quad (35)$$

Here, a_m^{-1} and b_m^{-1} are defined with respect to the *left* eigenvectors of the non-Hermitian matrix $\boldsymbol{L}_{0,m}$. Correspondingly, a_m and b_m describe the *right* eigenvectors:

$$a_m \equiv \frac{d_{-,m} - d_{+,m}}{\sqrt{2}}, \quad a_m^{-1} \equiv \frac{\sqrt{2}(\Gamma_{L,m}d_{-,m}^{\dagger} - \Gamma_{R,m}d_{+,m}^{\dagger})}{\Gamma_{L,m} + \Gamma_{R,m}}, \quad (36)$$

$$b_m^{-1} \equiv \frac{d_{-,m}^{\dagger} + d_{+,m}^{\dagger}}{\sqrt{2}}, \quad b_m \equiv \frac{\sqrt{2}(\Gamma_{R,m}d_{-,m} + \Gamma_{L,m}d_{+,m})}{\Gamma_{L,m} + \Gamma_{R,m}}. \quad (37)$$

These operators satisfy the anticommutation relations

$$\{a_m, a_{m'}^{-1}\} = \{b_m, b_{m'}^{-1}\} = \delta_{mm'}, \quad (38)$$

$$\{b_m, a_{m'}^{-1}\} = \{a_m, b_{m'}^{-1}\} = \{a_m, a_{m'}\} = \{b_m, b_{m'}\} = 0. \quad (39)$$

Since the eigenvalues of $\widehat{H}_{\text{eff}}^{(0)}$ are complex, the corresponding eigenstates show a decaying or explosive long-time behavior for $t \to \infty$:

$$a_m^{\mathcal{I}}(t) = a_m e^{(\Delta_m - i\xi_{d,m})t}, \quad b_m^{\mathcal{I}}(t) = b_m e^{-(\Delta_m + i\xi_{d,m})t}. \quad (40)$$

The relaxation time is determined by Δ_m, i.e., the imaginary part of the eigenvalue. Thus, the final and initial states in the time-dependent perturbation theory for correlation functions must satisfy a strong requirement that they should eliminate the explosive part, preserving only the decaying part. This condition is cleared by taking the states, in which all the explosive "a_m" particles are filled, as a set of "vacuums"

$$\langle\!\langle I\| \equiv \langle 0| \, a_N \, a_{N-1} \ldots a_2 \, a_1, \quad (41)$$

$$\|\rho\rangle\!\rangle \equiv a_1^{-1} \, a_2^{-1} \ldots a_{N-1}^{-1} \, a_N^{-1} \, |0\rangle. \quad (42)$$

These two states are normalized such that $\langle\!\langle I\|\rho\rangle\!\rangle = 1$. We can see that the causal propagators defined with respect to these states correctly describe the relaxation process

$$\langle\!\langle I\|\mathrm{T}\, a_m^{\mathcal{I}}(t)\, a_{m'}^{-1\mathcal{I}}(0)\|\rho\rangle\!\rangle = -\delta_{mm'}\,\theta(-t)\, e^{(\Delta_m - i\xi_{d,m})t}, \quad (43)$$

$$\langle\!\langle I\|\mathrm{T}\, b_m^{\mathcal{I}}(t)\, b_{m'}^{-1\mathcal{I}}(0)\|\rho\rangle\!\rangle = \delta_{mm'}\,\theta(t)\, e^{-(\Delta_m + i\xi_{d,m})t}. \quad (44)$$

The final state $\langle\!\langle I\|$ also satisfies the other requirement for the turnaround point of the Keldysh contour

$$\langle\!\langle I\|d_{-,m} = \langle\!\langle I\|d_{+,m}, \quad \langle\!\langle I\|d_{-,m}^{\dagger} = -\langle\!\langle I\|d_{+,m}^{\dagger}. \quad (45)$$

These relations hold for arbitrary m, and reproduce a linear dependence between the $-$ and $+$ components of the Keldysh correlation functions corresponding to Eqs. (76) and (77).

In the final and initial states, defined in Eqs. (41) and (42), the charge Q_m vanishes identically for each m of the orbitals:

$$\langle\!\langle I\|Q_m = 0, \quad Q_m\|\rho\rangle\!\rangle = 0. \quad (46)$$

It can also be deduced from this property that $\langle\!\langle I\|$ and $\|\rho\rangle\!\rangle$ are also the eigenstates for both $\widehat{H}_{\text{eff}}^{(0)}$ and $\widehat{H}_{\text{eff}}$, with zero eigenvalue,

$$\langle\!\langle I\|\widehat{H}_{\text{eff}}^{(0)} = 0, \quad \langle\!\langle I\|\widehat{H}_{\text{eff}} = 0, \quad (47)$$

$$\widehat{H}_{\text{eff}}^{(0)}\|\rho\rangle\!\rangle = 0, \quad \widehat{H}_{\text{eff}}\|\rho\rangle\!\rangle = 0. \quad (48)$$

Therefore, $\langle\!\langle I\|$ and $\|\rho\rangle\!\rangle$ do not evolve in time in both the Schrödinger and interaction representations

$$\langle\!\langle I\|\, e^{i\widehat{H}_{\text{eff}}t} = \langle\!\langle I\|, \quad \langle\!\langle I\|\widehat{\mathcal{U}}(t,t') = \langle\!\langle I\|, \quad (49)$$

$$e^{-i\widehat{H}_{\text{eff}}t}\|\rho\rangle\!\rangle = \|\rho\rangle\!\rangle, \quad \widehat{\mathcal{U}}(t,t')\|\rho\rangle\!\rangle = \|\rho\rangle\!\rangle. \quad (50)$$

Specifically, in the interaction representation, the initial condition is given formally at $t \to -\infty$. Therefore, taking the initial condition to be $\|\rho(-\infty)\rangle\!\rangle \equiv \|\rho\rangle\!\rangle$, the time evolution of the wave function in the interaction representation can be described in the form

$$\|\rho(t)\rangle\!\rangle \equiv \widehat{\mathcal{U}}(t, -\infty)\|\rho(-\infty)\rangle\!\rangle = \|\rho\rangle\!\rangle. \quad (51)$$

Then, the expectation values are defined with respect to the wave function at $t = 0$ that is the time the Heisenberg and the interaction representations coincide:

$$\langle\mathcal{O}(t)\rangle \equiv \langle\!\langle I\|\mathcal{O}(t)\|\rho(0)\rangle\!\rangle \quad (52)$$

$$= \langle\!\langle I\|\mathrm{T}\,\mathcal{O}^{\mathcal{I}}(t)\,\widehat{\mathcal{U}}(\infty, -\infty)\|\rho(-\infty)\rangle\!\rangle. \quad (53)$$

This completes an explicit construction of the time-dependent perturbation theory for the high bias limit.

B. Statistical distributions at $eV \to \infty$

The initial state $\|\rho\rangle\!\rangle$ determines the density matrix in the limit of $eV \to \infty$, and has the properties similar to Eq. (45):

$$\Gamma_{L,m}\, d_{+,m}\|\rho\rangle\!\rangle = -\Gamma_{R,m}\, d_{-,m}\|\rho\rangle\!\rangle, \quad (54)$$

$$\Gamma_{R,m}\, d_{+,m}^{\dagger}\|\rho\rangle\!\rangle = \Gamma_{L,m}\, d_{-,m}^{\dagger}\|\rho\rangle\!\rangle. \quad (55)$$

The underlying statistical weight can be extracted as a density matrix, defined such that $\widehat{\rho}\|I\rangle \equiv \|\rho\rangle$ [47],

$$\widehat{\rho} = \prod_{m=1}^{N}(1 + 2r_m\, q_m), \quad r_m \equiv \frac{\Gamma_{L,m} - \Gamma_{R,m}}{\Gamma_{L,m} + \Gamma_{R,m}}, \quad (56)$$

where $\|I\rangle\!\rangle$ is a conjugate of $\langle\!\langle I\|$ whose explicit form is given in the right-hand side of Eq. (41). This density matrix correctly describes the statistical distribution in the high bias limit. Note that $\widehat{\rho}$ in this case does not depend on the interaction $U_{mm'}$ but varies as a function of r_m that parametrizes the asymmetry in the dot-lead couplings. Specifically, in the symmetric-coupling case where $r_m = 0$ for all m, it describes a uniform distribution $\widehat{\rho} = 1$ and the average occupation of $n_{-,m}$ becomes the same as that of $n_{+,m}$.

The average formula (52) reproduces exactly the local charges in the high bias limit

$$\langle\!\langle I\|q_m\|\rho(0)\rangle\!\rangle = \frac{r_m}{2}, \quad (57)$$

and $\langle n_{-,m}\rangle + \langle n_{+,m}\rangle = 1$. Furthermore, the steady currents through the dot are also correctly reproduced:

$$\langle\!\langle I\|I_{R,m}\|\rho(0)\rangle\!\rangle = \langle\!\langle I\|I_{L,m}\|\rho(0)\rangle\!\rangle = \frac{2\Gamma_{L,m}\Gamma_{R,m}}{\Gamma_{L,m} + \Gamma_{R,m}}. \quad (58)$$

Note that the averages of the charges and currents do not depend on $U_{mm'}$ in the high bias limit. Similarly, the dynamic susceptibilities for charges and currents also take the noninteracting values as discussed in the next section.

V. CORRELATION FUNCTIONS IN THE THERMAL FIELD THEORY FOR $eV \to \infty$

In this section, we explain the relations between the Keldysh correlation functions and the corresponding thermal-field-theoretical ones. We also describe some important high bias properties.

A. Dynamic susceptibility

We consider a dynamic susceptibility, defined by

$$\chi_{mm'}^{\mu\nu}(t) \equiv -i\sum_{\lambda\lambda'}\tau_3^{\mu\lambda}\tau_3^{\lambda'\nu}\langle\!\langle I\|\mathrm{T}\,\delta n_{\lambda,m}(t)\,\delta n_{\lambda',m'}\|\rho\rangle\!\rangle, \quad (59)$$

where $\delta n_{\mu,m} \equiv n_{\mu,m} - \langle n_{\mu,m} \rangle$ for $\mu = -, +$. The Pauli matrix $\boldsymbol{\tau}_3$ has been multiplied so that each (μ, ν) component of $\chi_{mm'}^{\mu\nu}$ coincides with the corresponding element of the Keldysh susceptibility.

Equation (59) can be calculated further, rewriting it in terms of the relative charge $\delta q_m \equiv q_m - \langle q_m \rangle$:

$$\chi_{mm'}^{\mu\nu}(t) = -i \langle\langle I \| \mathrm{T} \, \delta q_m(t) \, \delta q_{m'}(0) \| \rho \rangle\rangle$$
$$= -i\theta(t) \langle\langle I \| \delta q_m \, e^{-i\widehat{H}_{\mathrm{eff}}t} \, \delta q_{m'} \| \rho \rangle\rangle$$
$$- i\theta(-t) \langle\langle I \| \delta q_{m'} \, e^{i\widehat{H}_{\mathrm{eff}}t} \, \delta q_m \| \rho \rangle\rangle. \quad (60)$$

We have used an identity $\delta n_{\mu,m} = \frac{1}{2} Q_m - \mathrm{sign}(\mu) \, \delta q_m$ and the high bias properties described in Eq. (46) to obtain the second line. This expression shows that the dynamics of the excited states $\langle\langle I \| \delta q_m$ and $\delta q_{m'} \| \rho \rangle\rangle$ determine the time evolution of $\chi_{mm'}^{\mu\nu}(t)$. In these two states, one particle-hole pair is excited, respectively, from the "vacuums" $\langle\langle I \|$ and $\| \rho \rangle\rangle$, by the matrix elements

$$\delta q_m = \frac{1}{2} \left(a_m^{-1} b_m + \frac{4\Gamma_{L,m}\Gamma_{R,m}}{\Delta_m^2} \, b_m^{-1} a_m \right)$$
$$+ \frac{r_m}{2} \left(a_m^{-1} a_m - b_m^{-1} b_m - 1 \right), \quad (61)$$

as

$$\langle\langle I \| \delta q_m = \frac{1}{2} \langle 0 | a_N \ldots a_{m+1} \, b_m \, a_{m-1} \ldots a_1, \quad (62)$$

$$\delta q_m \| \rho \rangle\rangle = \frac{2\Gamma_{L,m}\Gamma_{R,m}}{\Delta_m^2} \, a_1^{-1} \ldots a_{m-1}^{-1} \, b_m^{-1} \, a_{m+1}^{-1} \ldots \, a_N^{-1} \, | 0 \rangle . \quad (63)$$

The particle-hole-pair excitation does not change the total Q_m in the Liouville-Fock space, and thus

$$\langle\langle I \| \delta q_m \, Q_{m''} = 0, \quad Q_{m''} \, \delta q_{m'} \| \rho \rangle\rangle = 0 \quad (64)$$

for all $m'' (= 1, 2, \ldots, N)$. Therefore, in Eq. (60) the operators $Q_{m''}$'s included in $\widehat{H}_{\mathrm{eff}}$ in the intermediate states can be replaced by the corresponding eigenvalues $Q_{m''} = 0$ for all m'':

$$\chi_{mm'}^{\mu\nu}(t)$$
$$= -i\theta(t) \langle\langle I \| \delta q_m \, e^{-i \sum_{m''}(d_{m''}^\dagger L_{0,m''} d_{m''} - i\Delta_{m''})t} \delta q_{m'} \| \rho \rangle\rangle$$
$$- i\theta(-t) \langle\langle I \| \delta q_{m'} \, e^{i \sum_{m''}(d_{m''}^\dagger L_{0,m''} d_{m''} - i\Delta_{m''})t} \delta q_m \| \rho \rangle\rangle, \quad (65)$$

and thus the interaction term vanishes in the intermediate states, Consequently, the dynamic susceptibility is asymptotically free in the high bias limit as it coincides with the noninteracting form

$$\chi_{mm'}^{\mu\nu}(t) = -i \, \delta_{mm'} \, \frac{\Gamma_{L,m}\Gamma_{R,m}}{(\Gamma_{L,m} + \Gamma_{R,m})^2} \, e^{-2\Delta_m|t|}. \quad (66)$$

Alternatively, one can calculate $\chi_{mm'}^{\mu\nu}(t)$ from the equation of motion, in which the decay rate $2\Delta_m$ appears as the eigenvalue of $\mathcal{L}_m^2$, mentioned in Sec. III B.

This asymptotically free behavior in the high bias limit is common to a wide class of the correlation functions $X_{AB}(t,t')$, defined with respect to the operators A and B which commute with Q_m for all m:

$$X_{AB}(t,t') \equiv -i \langle\langle I \| \mathrm{T} \, A(t) \, B(t') \| \rho(0) \rangle\rangle, \quad (67)$$

$$[A \, , \, Q_m] = [B \, , \, Q_m] = 0. \quad (68)$$

For this correlation function, the relations corresponding to Eq. (64) follow for both A and B from the condition (68), and thus the interaction effects vanish as that in the case of the dynamic susceptibility $\chi_{mm'}^{\mu\nu}(t)$. One important example of this is the shot noise that can be derived from the current-current correlation function. Because the current operator $I_{\alpha,m}$ satisfies a commutation relation $[I_{\alpha,m} \, , \, Q_m] = 0$, the high bias asymptotic form of the ω-dependent current fluctuations becomes identical to the noninteracting result also in the multiorbital case as that in the $N = 2$ case [26].

B. Green's function

We next describe the correspondence between the Keldysh Green's function and the ones defined with respect to the Liouville-Fock space. The free Green's function for $\widehat{H}_{\mathrm{eff}}^{(0)}$ is defined by

$$\mathcal{G}_{0,m}^{\mu\nu}(t) \equiv -i \langle\langle I \| \mathrm{T} \, d_{\mu,m}^{\mathcal{I}}(t) \, d_{\nu,m}^{\dagger\mathcal{I}}(0) \| \rho \rangle\rangle. \quad (69)$$

This function can be calculated, using Eqs. (40) and (41),

$$\boldsymbol{\mathcal{G}}_{0,m} \equiv \begin{bmatrix} \mathcal{G}_{0,m}^{--} & \mathcal{G}_{0,m}^{-+} \\ \mathcal{G}_{0,m}^{+-} & \mathcal{G}_{0,m}^{++} \end{bmatrix} = \boldsymbol{G}_{0,m} \, \boldsymbol{\tau}_3. \quad (70)$$

Here, $\boldsymbol{G}_{0,m}(\omega)$ is the high bias asymptotic form of the Keldysh Green's function

$$\{\boldsymbol{G}_{0,m}(\omega)\}^{-1} = \boldsymbol{\tau}_3 \, [(\omega - \xi_{d,m})\boldsymbol{1} - \boldsymbol{L}_0]. \quad (71)$$

Note that $\varepsilon_{d,m}$ which appeared in the original definition of $\boldsymbol{G}_{0,m}(\omega)$ given in Eq. (7) has been replaced by $\xi_{d,m}$, including the energy shift defined in Eq. (18) into the nonperturbed part.

The interacting Green's function for the Liouville-Fock space is defined by

$$\mathcal{G}_m^{\mu\nu}(t) \equiv -i \langle\langle I \| \mathrm{T} \, d_{\mu,m}(t) \, d_{\nu,m}^\dagger(0) \| \rho(0) \rangle\rangle \quad (72)$$
$$= -i \langle\langle I \| \mathrm{T} \, d_{\mu,m}^{\mathcal{I}}(t) \, d_{\nu,m}^{\dagger\mathcal{I}}(0) \, \widehat{\mathcal{U}}(\infty, -\infty) \| \rho \rangle\rangle. \quad (73)$$

The same relation holds between the interacting Green's functions $\boldsymbol{\mathcal{G}}_m$ and $\boldsymbol{G}_m$ as that in the noninteracting case

$$\boldsymbol{\mathcal{G}}_m = \boldsymbol{G}_m \, \boldsymbol{\tau}_3. \quad (74)$$

This can be verified perturbatively, using the Feynman diagrammatic expansion which can be generated from $\widehat{\mathcal{U}}(\infty, -\infty)$ defined in Eq. (73). The noninteracting Green's function $\boldsymbol{\mathcal{G}}_{0,m}$ that is assigned to the Feynman diagrams has one-to-one correspondence with the Keldysh propagator $\boldsymbol{G}_{0,m}$, as shown in Eq. (70). Furthermore, the Feynman rule for $\boldsymbol{\mathcal{G}}_m$ is essentially the same as that for $\boldsymbol{G}_m$ in the Keldysh formalism. There is a slight difference in the treatment of the Hartree term but the counter term, which is a part of $\widehat{H}_{\mathrm{eff}}$, compensates the difference as shown in Appendix A. Therefore, there is an exact diagram-to-diagram correspondence between the Keldysh and thermal-field-theoretical perturbation expansion, and thus Eq. (74) holds. Note that the sign that arises from $\boldsymbol{\tau}_3$ also appears in the relation between the Keldysh self-energy

Σ_m for G_m and the corresponding self-energy Σ_m^{TFT}, defined by $\{\mathcal{G}_m\}^{-1} = \{\mathcal{G}_{0,m}\}^{-1} - \Sigma_m^{\text{TFT}}$, as

$$\Sigma_m(\omega) = \tau_3 \Sigma_m^{\text{TFT}}(\omega). \tag{75}$$

The four components of $\mathcal{G}_m^{\mu\nu}$ have the same linear dependence as the Keldysh components $G_m^{\mu\nu}$ have. Therefore, the retarded G_m^r and advanced G_m^a Green's functions can be expressed in two different forms

$$G_m^r = \mathcal{G}_m^{--} + \mathcal{G}_m^{-+} = \mathcal{G}_m^{+-} + \mathcal{G}_m^{++}, \tag{76}$$

$$G_m^a = \mathcal{G}_m^{--} - \mathcal{G}_m^{+-} = \mathcal{G}_m^{++} - \mathcal{G}_m^{-+}. \tag{77}$$

In the high bias limit, $\mathcal{G}_m$ can be expressed in terms of these two Green's functions

$$\mathcal{G}_m = \frac{G_m^r}{\Delta_m} \begin{bmatrix} \Gamma_{R,m} & \Gamma_{L,m} \\ \Gamma_{R,m} & \Gamma_{L,m} \end{bmatrix} + \frac{G_m^a}{\Delta_m} \begin{bmatrix} \Gamma_{L,m} & -\Gamma_{L,m} \\ -\Gamma_{R,m} & \Gamma_{R,m} \end{bmatrix}. \tag{78}$$

This is because the statistical distribution for $eV \to \infty$ is determined by a time-independent state $\|\rho\rangle\rangle$ as shown in Eqs. (54)–(56). Furthermore, only a single component among the four is independent since the relation $G_m^a(\omega) = \{G_m^r(\omega)\}^*$ holds in the frequency representation. For this reason, we consider mainly the retarded Green's function in the rest of the paper.

VI. EXACT INTERACTING GREEN'S FUNCTION FOR $eV \to \infty$

In this section, we describe a derivation of the asymptotic form of Green's function in the high bias limit.

A. Generic form in the high bias limit

The retarded Green's function can be expressed in the following form, using Eq. (76):

$$G_m^r(t) = \tfrac{1}{2}(\mathcal{G}_m^{--}(t) + \mathcal{G}_m^{-+}(t) + \mathcal{G}_m^{+-}(t) + \mathcal{G}_m^{++}(t)) \tag{79}$$

$$= -i\,\theta(t)\,\tfrac{1}{2}\,\langle\langle I \| (d_{-,m}(t) + d_{+,m}(t))$$

$$\times\,(d_{-,m}^\dagger + d_{+,m}^\dagger)\|\rho(0)\rangle\rangle. \tag{80}$$

This can be rewritten further, using the properties of $\langle\langle I \|$ and $\|\rho\rangle\rangle$ given in Eqs. (47) and (48),

$$G_m^r(t) = -i\,\theta(t)\,\langle\langle I_m \| e^{-i\widehat{H}_{\text{eff}}t}\|\rho_m\rangle\rangle. \tag{81}$$

Here, $\langle\langle I_m \|$ and $\|\rho_m\rangle\rangle$ denote the intermediate states with single-particle excitations

$$\langle\langle I_m \| \equiv \langle\langle I \| \frac{1}{\sqrt{2}}(d_{-,m} + d_{+,m})$$

$$= (-1)^{m-1}\,\langle 0|\,a_N\,\ldots\,a_{m+1}\,d_{-,m}d_{+,m}\,a_{m-1}\ldots a_1, \tag{82}$$

$$\|\rho_m\rangle\rangle \equiv \frac{1}{\sqrt{2}}(d_{-,m}^\dagger + d_{+,m}^\dagger)\|\rho\rangle\rangle$$

$$= (-1)^{m-1}\,a_1^{-1}\ldots a_{m-1}^{-1}\,d_{+,m}^\dagger d_{-,m}^\dagger\,a_{m+1}^{-1}\ldots\,a_N^{-1}|0\rangle. \tag{83}$$

In contrast to the particle-hole-pair excitation for the dynamic susceptibilities described in Eqs. (62) and (63), in the single-particle states $\langle\langle I_m \|$ and $\|\rho_m\rangle\rangle$ the orbital m is doubly occupied while all the other orbitals $m'\,(\neq m)$ are kept unchanged in a similar way. Thus, for $\widehat{H}_{\text{eff}}$ which determines time evolution of the intermediate state described in Eq. (81), the operators $Q_{m'}$'s can be replaced by their eigenvalues: $Q_m = 1$ and $Q_{m'} = 0$ for $m' \neq m$. This significantly simplifies Eq. (81), and makes the correlation effects factorizable in a bilinear form

$$G_m^r(t) = -i\,\theta(t)\,e^{-i(\xi_{d,m}-i\Delta_m)t}\prod_{m'(\neq m)} e^{-\Delta_{m'}t}\,\langle\langle I_m \| e^{-i\,d_{m'}^\dagger \widetilde{L}_{m'}^{(m)} d_{m'} t}\|\rho_m\rangle\rangle, \tag{84}$$

$$\widetilde{L}_{m'}^{(m)} \equiv i \begin{bmatrix} \Gamma_{L,m'} - \Gamma_{R,m'} - i\,\tfrac{1}{2}\,U_{m'm} & -2\Gamma_{L,m'} \\ -2\Gamma_{R,m'} & -(\Gamma_{L,m'} - \Gamma_{R,m'}) + i\,\tfrac{1}{2}\,U_{m'm} \end{bmatrix}. \tag{85}$$

The matrix $\widetilde{L}_{m'}^{(m)}$ consists of the free part L_0 defined in Eq. (13) and the correction due to the interelectron interaction. The product in Eq. (84) can be calculated separately for each $m'\,(\neq m)$ as

$$\langle\langle I_m \| e^{-i\,d_{m'}^\dagger \widetilde{L}_{m'}^{(m)} d_{m'} t}\|\rho_m\rangle\rangle = \begin{bmatrix} 1 & -1 \end{bmatrix} e^{-i\,\widetilde{L}_{m'}^{(m)}t} \begin{bmatrix} \frac{\Gamma_{L,m}}{\Delta_m} \\ -\frac{\Gamma_{R,m}}{\Delta_m} \end{bmatrix} = Z_{m'}^{(m+)}\,e^{-i\mathcal{E}_{m'}^{(m)}t} + Z_{m'}^{(m-)}\,e^{i\mathcal{E}_{m'}^{(m)}t}. \tag{86}$$

Here, $\mathcal{E}_{m'}^{(m)}$ is a complex eigenvalue of $\widetilde{L}_{m'}^{(m)}$ and $Z_{m'}^{(m\pm)}$ is a weight factor determined by the corresponding eigenvector [45]

$$Z_{m'}^{(m\pm)} \equiv \frac{1}{2}\left(1 \pm \frac{i\Delta_{m'} + \frac{r_{m'}}{2}\,U_{m'm}}{\mathcal{E}_{m'}^{(m)}}\right), \quad \mathcal{E}_{m'}^{(m)} \equiv \sqrt{\frac{1}{4}\,U_{m'm}^2 - \Delta_{m'}^2 + ir_{m'}\Delta_{m'}\,U_{m'm}}. \tag{87}$$

We obtain the explicit expression of the retarded Green's function, substituting Eq. (86) into Eq. (84),

$$G_m^r(t) = -i\,\theta(t)\,e^{-i(\xi_{d,m}-i\Delta_m)t}\prod_{m'(\neq m)} e^{-\Delta_{m'}t}\left(Z_{m'}^{(m+)}\,e^{-i\mathcal{E}_{m'}^{(m)}t} + Z_{m'}^{(m-)}\,e^{i\mathcal{E}_{m'}^{(m)}t}\right). \tag{88}$$

This is a main result of this work, and the Green's function can be written in a factorized form in the time representation.

The asymptotically exact result for $eV \to \infty$ captures essential physics of relaxation of interacting electrons at high-energy scales. The imaginary part of $\mathcal{E}_{m'}^{(m)}$ is bounded in the range $|\operatorname{Im} \mathcal{E}_{m'}^{(m)}| \leqslant \Delta_{m'}$, and it certifies that $G_m^r(t)$ decays at long time [45]. The squared eigenvalue $\{\mathcal{E}_{m'}^{(m)}\}^2$ also corresponds to the eigenvalue of the operator $\mathcal{L}_m^2$ for $\widehat{(UQ)_m} = U_{m'm}$, which is defined in Eq. (31). This means that the particle-hole-pair excitation in the intermediate state evolves in time and contributes to the relaxations, which we can see more clearly in the continued-fraction representation in the next section. Note that the high bias expression (88) in the symmetric-coupling case, where $r_{m''} = 0$ for all m'', can also be regarded as an exact high-temperature Green's function at equilibrium because of the relation described in Eq. (11). The Fourier transform $G_m^r(\omega) = \int_0^\infty dt\, e^{i(\omega+i0^+)t}\, G_m^r(t)$, which can be carried out by expanding the product, becomes a function of $\omega_m \equiv \omega - \xi_{d,m}$ in the frequency representation. Alternatively, it can also be calculated, using a resolvent form of Eq. (81),

$$G_m^r(\omega) = \langle\!\langle I_m \| \frac{1}{\omega - \widehat{H}_{\text{eff}} + i0^+} \| \rho_m \rangle\!\rangle. \quad (89)$$

B. Some special cases

We examine some special cases in this section. The first one is the free-particle limit where $\widehat{H}_{\text{eff}}^{(U)} \to 0$. Equation (88) obviously reproduces the free propagator

$$G_{0,m}^r(t) = -i\,\theta(t)\, e^{-i(\xi_{d,m} - i\Delta_m)t} \quad (90)$$

as $e^{-\Delta_{m'}t} \langle\!\langle I_m \| e^{-i\, d_{m'}^\dagger \widehat{L}_{m'}^{(m)} d_{m'} t} \| \rho_m \rangle\!\rangle \to 1$ for $m' \neq m$ in the noninteracting case.

The second example is the case where one of the two leads are disconnected. In the limit $r_{m''} \to +1\,(-1)$ for all m'', the right (left) lead is disconnected, and the impurity level with the width $\Delta_m \to \Gamma_{L,m}\,(\Gamma_{R,m})$ is fully occupied (empty). Then, the Green's function takes the form

$$\lim_{\{r_{m''}\} \to \pm 1} G_m^r(t) = -i\,\theta(t)\, e^{-i\left(\xi_{d,m} \pm \frac{N-1}{2}\overline{U}_m - i\Delta_m\right)t}. \quad (91)$$

The corresponding spectral function for $r_{m''} \to \pm 1$ has a single Lorentzian peak at $\omega = \xi_{d,m} \pm (N-1)\overline{U}_m/2$ with

$\overline{U}_m \equiv \sum_{m'(\neq m)} U_{m'm}/(N-1)$. Note that the peak position depends on which of the leads, R or L, is disconnected.

The third one is the atomic limit, where both $\Gamma_{L,m''}$ and $\Gamma_{R,m''}$ vanish for all m''. In this case, the complex eigenvalue and weight factors approach $\mathcal{E}_{m'}^{(m)} \to U_{m'm}/2$ and $Z_{m'}^{(m\pm)} \to \frac{1}{2}$. Then, Eq. (88) takes the form

$$\lim_{\substack{\{\Gamma_{R,m''}\} \to 0 \\ \{\Gamma_{L,m''}\} \to 0}} G_m^r(t)$$

$$= -i\,\theta(t)\, e^{-i\xi_{d,m}t} \prod_{m'(\neq m)} \frac{e^{-i\frac{1}{2}U_{m'm}t} + e^{i\frac{1}{2}U_{m'm}t}}{2}. \quad (92)$$

VII. GREEN'S FUNCTION FOR THE UNIFORM INTERACTION CASE

In this section, we consider the high bias Green's function for the m-independent interactions and hybridizations, choosing $U_{mm'} = U$, $\Delta_m = \Delta$, and $r_m = r$ for all m and m'. However, the impurity levels $\xi_{d,m} = \varepsilon_{d,m} + (N-1)U/2$ can still be dependent on m, and also the coupling can be asymmetric $\Gamma_L \neq \Gamma_R$. Then, Eq. (88) takes the form

$$G_m^r(t) = -i\,\theta(t)\, e^{-i(\xi_{d,m} - iN\Delta)t} \left(Z^{(+)} e^{-i\mathcal{E}t} + Z^{(-)} e^{i\mathcal{E}t} \right)^{N-1}. \quad (93)$$

Here, $\mathcal{E}$ and $Z^{(\pm)}$ correspond to $\mathcal{E}_{m'}^{(m)}$ and $Z_{m'}^{(m\pm)}$ for the uniform parameters, respectively. This Green's function can be rewritten in a partial fraction form, carrying out the Fourier transform using the binominal expansion

$$G_m^r(\omega) = \sum_{\mathcal{Q}=0}^{N-1} \binom{N-1}{\mathcal{Q}} \frac{\{Z^{(+)}\}^{\mathcal{Q}} \{Z^{(-)}\}^{N-1-\mathcal{Q}}}{\omega - \xi_{d,m} + iN\Delta + (N-1-2\mathcal{Q})\mathcal{E}}. \quad (94)$$

Note that the imaginary part of $G_m^r(\omega)$ is determined not only by $iN\Delta$ in the denominator but also through the complex parameters $\mathcal{E}$ and $Z^{(\pm)}$.

A. Continued-fraction representation

The Green's function can also be expressed in a continued-fraction form, converting Eq. (94) or carrying out the Householder transformation for Eq. (89):

$$G_m^r(\omega) = \cfrac{1}{\omega_m - \mathcal{A}_1 \frac{rU}{2} + i\,\mathcal{C}_1\Delta - \cfrac{\mathcal{B}_1(1-r^2)\left(\frac{U}{2}\right)^2}{\omega_m - \mathcal{A}_2\frac{rU}{2} + i\,\mathcal{C}_2\Delta - \cfrac{\mathcal{B}_2(1-r^2)\left(\frac{U}{2}\right)^2}{\ddots - \cfrac{\ddots}{\omega_m - \mathcal{A}_{N-1}\frac{rU}{2} + i\,\mathcal{C}_{N-1}\Delta - \cfrac{\mathcal{B}_{N-1}(1-r^2)\left(\frac{U}{2}\right)^2}{\omega_m - \mathcal{A}_N\frac{rU}{2} + i\,\mathcal{C}_N\Delta}}}}}, \quad (95)$$

where $\omega_m = \omega - \xi_{d,m}$. The square-root dependence due to $\mathcal{E}$ disappears in the continued-fraction representation as the coefficients $\mathcal{A}_k$, $\mathcal{B}_k$, and $\mathcal{C}_k$ (for $k = 1, 2, \ldots, N$) are integers, which do not depend on the physical parameters

$$\mathcal{A}_k = N - 1 - 2(k-1), \quad \mathcal{B}_k = k(N-k),$$
$$\mathcal{C}_k = 2k - 1. \quad (96)$$

The coefficient $\mathcal{A}_k$, which determines the energy shifts due to the coupling asymmetry, decreases as k increases and changes the sign at the middle of k between 1 and N. The coefficient $\mathcal{B}_k$ corresponds to the residue of intermediate states with k particle-hole pairs, and has a maximum at the middle of k. In contrast, the coefficient $\mathcal{C}_k$ increases linearly with k. It determines the relaxation rate in the high bias limit, and can be

decomposed into two parts $\mathcal{C}_k \Delta = (k-1)2\Delta + \Delta$. The first term can be interpreted as a sum of the damping rate of $k-1$ intermediate particle-hole pairs, each of which decays with the ratio of 2Δ as mentioned in Secs. III B and V A, and the second term Δ corresponds to the decay rate of the single incident particle. Note that the initial part of the continued fraction (95) can be expressed in the form

$$\omega_m - \mathcal{A}_1 \frac{rU}{2} + i\,\mathcal{C}_1\,\Delta \;=\; \omega - \epsilon_{d,m} - \langle n_{m'} \rangle\,(N-1)U + i\Delta. \tag{97}$$

Here, the third term in the right-hand side corresponds to the energy shift due to the Hartree term with $\langle n_{m'} \rangle = (1+r)/2$, the average occupation of the orbital m' ($\neq m$). Therefore, the remainder part of the energy denominator can be regarded as

the self-energy correction $\Sigma_{d,m}^r(\omega)$ beyond the Hartree term

$$G_m^r(\omega) = \frac{1}{\omega - \epsilon_{d,m} - \langle n_{m'} \rangle\,(N-1)U + i\Delta - \Sigma_{d,m}^r(\omega)}. \tag{98}$$

In order to see these features of the Green's function more clearly, we provide some examples for first few N. In the simplest case, for $N=2$, it takes the form [26]

$$G_m^r(\omega)\big|_{N=2} \;=\; \frac{1}{\omega_m - \frac{rU}{2} + i\Delta - \frac{(1-r^2)\left(\frac{U}{2}\right)^2}{\omega_m + \frac{rU}{2} + i3\Delta}}. \tag{99}$$

For $N=3$,

$$G_m^r(\omega)\big|_{N=3} \;=\; \frac{1}{\omega_m - 2\frac{rU}{2} + i\Delta - \dfrac{2(1-r^2)\left(\frac{U}{2}\right)^2}{\omega_m + i3\Delta - \dfrac{2(1-r^2)\left(\frac{U}{2}\right)^2}{\omega_m + 2\frac{rU}{2} + i5\Delta}}}. \tag{100}$$

For $N=4$,

$$G_m^r(\omega)\big|_{N=4} \;=\; \frac{1}{\omega_m - 3\frac{rU}{2} + i\Delta - \dfrac{3(1-r^2)\left(\frac{U}{2}\right)^2}{\omega_m - \frac{rU}{2} + i3\Delta - \dfrac{4(1-r^2)\left(\frac{U}{2}\right)^2}{\omega_m + \frac{rU}{2} + i5\Delta - \dfrac{3(1-r^2)\left(\frac{U}{2}\right)^2}{\omega_m + 3\frac{rU}{2} + i7\Delta}}}}. \tag{101}$$

For $N=5$,

$$G_m^r(\omega)\big|_{N=5} \;=\; \frac{1}{\omega_m - 4\frac{rU}{2} + i\Delta - \dfrac{4(1-r^2)\left(\frac{U}{2}\right)^2}{\omega_m - 2\frac{rU}{2} + i3\Delta - \dfrac{6(1-r^2)\left(\frac{U}{2}\right)^2}{\omega_m + i5\Delta - \dfrac{6(1-r^2)\left(\frac{U}{2}\right)^2}{\omega_m + 2\frac{rU}{2} + i7\Delta - \dfrac{4(1-r^2)\left(\frac{U}{2}\right)^2}{\omega_m + 4\frac{rU}{2} + i9\Delta}}}}}. \tag{102}$$

For $N=6$,

$$G_m^r(\omega)\big|_{N=6} = \frac{1}{\omega_m - 5\frac{rU}{2} + i\Delta - \dfrac{5(1-r^2)\left(\frac{U}{2}\right)^2}{\omega_m - 3\frac{rU}{2} + i3\Delta - \dfrac{8(1-r^2)\left(\frac{U}{2}\right)^2}{\omega_m - \frac{rU}{2} + i5\Delta - \dfrac{9(1-r^2)\left(\frac{U}{2}\right)^2}{\omega_m + \frac{rU}{2} + i7\Delta - \dfrac{8(1-r^2)\left(\frac{U}{2}\right)^2}{\omega_m + 3\frac{rU}{2} + i9\Delta - \dfrac{5(1-r^2)\left(\frac{U}{2}\right)^2}{\omega_m + 5\frac{rU}{2} + i11\Delta}}}}}}. \tag{103}$$

These expressions are simplified further for $r=0$, i.e., the symmetric couplings or the high-temperature limit of thermal equilibrium, as all the terms corresponding to the energy shift vanish. Particularly for $N=2$, the exact self-energy becomes identical to the order U^2 results [25]. However, the similar cancellations of the higher-order terms in the power series of U do not occur for $N > 2$. This is because the high-order processes of the multiple particle-hole-pair

excitations occurring in different orbitals contribute to the self-energy for $N > 2$.

B. Spectral functions for the uniform interactions

We examine further the high bias property in the case of the uniform interactions. One of the simplest situations is the atomic limit where both Γ_L and Γ_R vanish. In this case, the

complex eigenvalue and weight factor become $\mathcal{E} \to U/2$ and $Z^{(\pm)} \to \frac{1}{2}$, respectively, as mentioned in Sec. VI B. Thus, the high bias retarded Green's function given in Eq. (94) simplifies

$$G_m^r(\omega)$$

$$\xrightarrow{\Gamma_{L/R} \to 0} \sum_{\mathcal{Q}=0}^{N-1} \binom{N-1}{\mathcal{Q}} \frac{1}{2^{N-1}} \frac{1}{\omega - \xi_{d,m} - \left(\mathcal{Q} - \frac{N-1}{2}\right)U}$$

$$= \frac{1}{\omega - \xi_{d,m} - \Sigma_{d,m}^{(\mathrm{ATM})}(\omega)}. \tag{104}$$

The Green's function in this limit has poles at $\omega = \xi_{d,m} + [\mathcal{Q} - (N-1)/2]U$ for $\mathcal{Q} = 0, 1, \ldots, N-1$, the residues of which are given by the binominal distribution. Each of these N poles represents contributions of a single-particle and a single-hole excitation between the $\mathcal{Q}$-particle and $\mathcal{Q}+1$-particle states. This assignment of the spectrum can be verified, comparing with the equilibrium finite-temperature Green's function in the atomic limit, given in Appendix B. The last line of Eq. (104) defines the $T \to \infty$ atomic-limit self-energy $\Sigma_{d,m}^{(\mathrm{ATM})}(\omega)$, the explicit form of which can be obtained from $\Sigma_{d,m}^r(\omega)$ that is defined in Eqs. (95) and (98) taking the limit of $\Delta \to 0$ and $r \to 0$,

The couplings to the leads Γ_L and Γ_R make these poles resonances with finite width. The Hubbard I (or Hubbard II for $N > 2$) approximation [40,48], or the decoupling approximation of equation of motion (EOM), gives the imaginary part $i\Delta$ to the atomic-limit Green's function defined in Eq. (104). Specifically, in the limit of $r \to 0$ or high-temperature limit $T \to \infty$, it appears only in the initial part of the continued-fraction expansion

$$G_m^{r(\mathrm{EOM})}(\omega) = \frac{1}{\omega - \xi_{d,m} + i\Delta - \Sigma_{d,m}^{(\mathrm{ATM})}(\omega)}. \tag{105}$$

Alternatively, $G_m^{r(\mathrm{EOM})}(\omega)$ can be expressed in a continued-fraction form similar to Eq. (95), by replacing the coefficients $\mathcal{C}_k$ such that $\mathcal{C}_1 \to 1$ for $k = 1$ and $\mathcal{C}_k \to 0$ for all the other k ($\geqslant 2$). This indicates that the decoupling approximation of EOM significantly underestimates the relaxation effects, especially for $N \gg 2$.

We also examine the NCA, which deals with the hybridizations in a more improved way. Specifically, in the limit of $T \to \infty$ at equilibrium $eV = 0$, the NCA equations for finite U can be solved analytically as shown in Appendix C, and then the retarded Green's function takes the form

$$G_m^{r(\mathrm{NCA})}(\omega) \xrightarrow{T \to \infty} \sum_{\mathcal{Q}=0}^{N-1} \binom{N-1}{\mathcal{Q}} \frac{1}{2^{N-1}}$$

$$\times \frac{1}{\omega - \xi_{d,m} - \left(\mathcal{Q} - \frac{N-1}{2}\right)U + iN\Delta}$$

$$= \frac{1}{\omega - \xi_{d,m} + iN\Delta - \Sigma_{d,m}^{(\mathrm{ATM})}(\omega + iN\Delta)}. \tag{106}$$

Note that the NCA in this case takes into account all possible 2^N impurity configurations, from the empty to the fully occupied orbital states [19]. In Eq. (106), the partial-fraction representation shows that the spectral function is given by

a series of the Lorentzian peaks with the same width $N\Delta$. The last line shows that, through the atomic-limit self-energy $\Sigma_{d,m}^{(\mathrm{ATM})}$ with the argument $\omega + iN\Delta$, the constant imaginary part $iN\Delta$ also appears in each step of the continued-fraction expansion. The explicit expression corresponding to Eq. (95) can be obtained by replacing the coefficients such that $\mathcal{C}_k \to N$ for all k and taking $r \to 0$ as mentioned. Note that the exact coefficient $\mathcal{C}_k = 2k - 1$ given in Eq. (96) shows that the imaginary part evolves step by step from $i\Delta$ to $i(2N-1)\Delta$ in the continued-fraction expansion. Therefore, the constant imaginary part of $iN\Delta$ that the NCA gives in the limit of $T \to \infty$ corresponds to an average of the exact ones.

In Fig. 2, the high bias spectral function $-\mathrm{Im}\,G_m^r(\omega)$ for $N = 4$ is plotted for some different values of r, choosing the interactions such that (a) $U/(\pi\Delta) = 2.0$ and (b) 4.0. Four separate peaks, emerging at $\omega - \xi_{d,m} = \pm U/2$ and $\pm 3U/2$, can be recognized in Fig. 2(b) for symmetric coupling $r = 0$. As the coupling asymmetry r increases, spectral weight moves towards a region around the right-end peak at $\omega - \xi_{d,m} = (N-1)U/2$ and in the limit of $r \to 1$ it takes the Lorentzian form with the width Δ which corresponds to Eq. (91). For negative r, the spectral weight moves in the opposite direction towards the left-end peak at $\omega - \xi_{d,m} = -(N-1)U/2$. Note that the impurity level is fully occupied for $r \to 1$, or empty for $r \to -1$, in the case where one of the leads is disconnected. For weak interactions, the level broadening due to the hybridizations dominates and the fine structure of the spectrum is smeared as seen in Fig. 2(a).

Figure 3 shows another example for even N ($= 6$) case: (a) $U/(\pi\Delta) = 2.0$ and (b) 6.0. The six-peak spectral structure can be seen at $\omega - \xi_{d,m} = \pm U/2$, $\pm 3U/2$, and $\pm 5U/2$ for
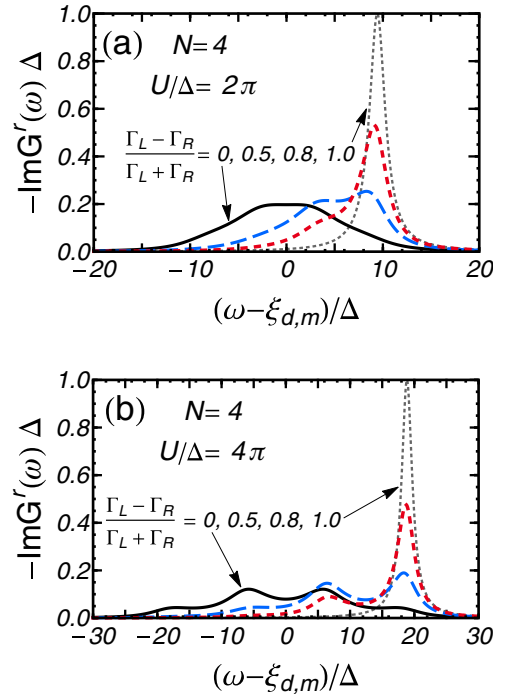

FIG. 2. (Color online) Exact high bias spectral function for $N = 4$ for uniform interactions (a) $U/(\pi\Delta) = 2.0$ and (b) 4.0, for different coupling asymmetries $r \equiv (\Gamma_L - \Gamma_R)/(\Gamma_L + \Gamma_R)$.
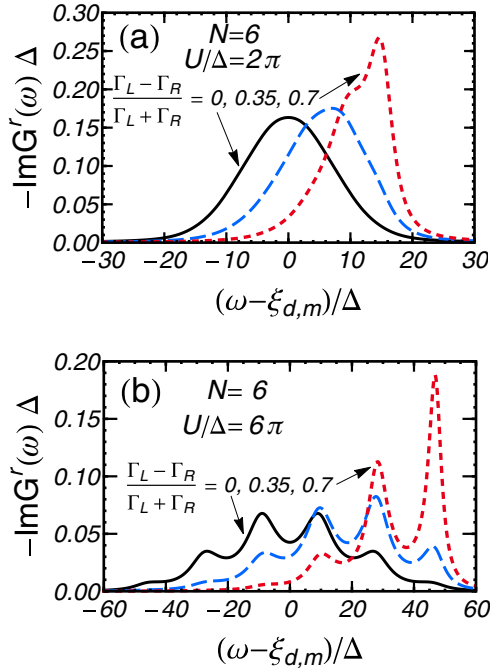
FIG. 3. (Color online) Exact high bias spectral function for $N = 6$ for uniform interactions (a) $U/(\pi \Delta) = 2.0$ and (b) 6.0, for different coupling asymmetries $r \equiv (\Gamma_L - \Gamma_R)/(\Gamma_L + \Gamma_R)$.

FIG. 4. (Color online) Exact high bias spectral function for odd N and uniform interactions: (a) $N = 3$, $U/(\pi \Delta) = 4.0$, and (b) $N = 5$, $U/(\pi \Delta) = 6.0$, for different coupling asymmetries $r \equiv (\Gamma_L - \Gamma_R)/(\Gamma_L + \Gamma_R)$.

symmetric coupling $r = 0$ in Fig. 3(b). As the coupling asymmetry r increases, the spectral weight moves towards the higher-energy region, as mentioned in the above. Specifically, the results obtained at $r = 0.7$ show a transient behavior that the highest two peaks share the most of the spectral weight. For weak interactions, as seen in Fig. 3(a), not all the six peaks emerge in a distinguishable way because of the level broadening due to the coupling to the leads.

The other examples, shown in Fig. 4, are the spectral function for odd N with (a) $N = 3$, $U/(\pi \Delta) = 4.0$, and (b) $N = 5$, $U/(\pi \Delta) = 6.0$. In the case of odd N, one of the peaks appears at the center where $\omega - \xi_{d,m} = 0$. The central peak corresponds to the excitations between the $\mathcal{Q} = (N - 1)/2$ and $(N + 1)/2$ particle states, and it is nothing to do with the Kondo singlet state. The asymmetry in the couplings also shifts the spectral weight to the higher-energy region as that in the even-N case.

The asymptotically exact Green's function can also be used as a standard for comparisons to check out the accuracy, or applicability, of theoretical calculations. Figure 5 compares the exact high-temperature results (solid line) and the NCA results of the spectral function for the SU(4) particle-hole-symmetric case $\varepsilon_d = -3U/2$ at equilibrium $eV = 0$. The NCA results are obtained (dotted line) at $T = T_K$ and (dashed line) at $T \to \infty$ from Eq. (106). The Kondo temperature is defined by $T_K = \pi z \Delta/4$ with z, the wave function renormalization factor that has been deduced from the NRG: (a) $z = 0.52$ for $U/(\pi \Delta) = 2.0$, and (b) $z = 0.25$ for $U/(\pi \Delta) = 4.0$. We see that the high-temperature NCA results (dashed line) for strong interactions, shown in Fig. 5(b), reasonably agree with the exact results, specifically at $6.0 \lesssim |\omega|/\Delta \lesssim 12.0$ between the lowest and the next peaks. However, the NCA underestimates
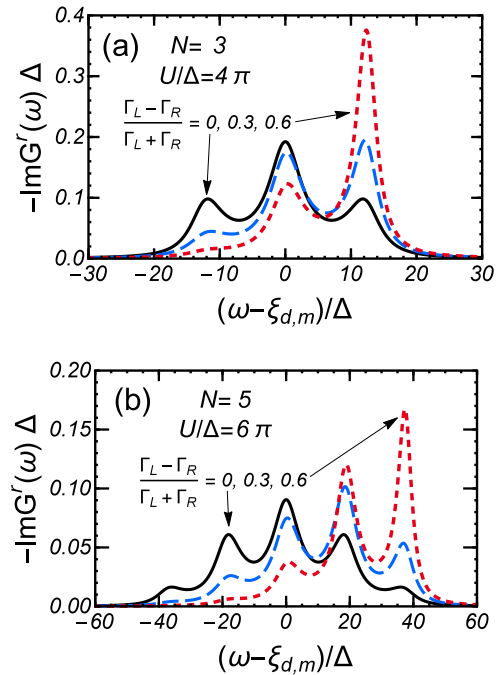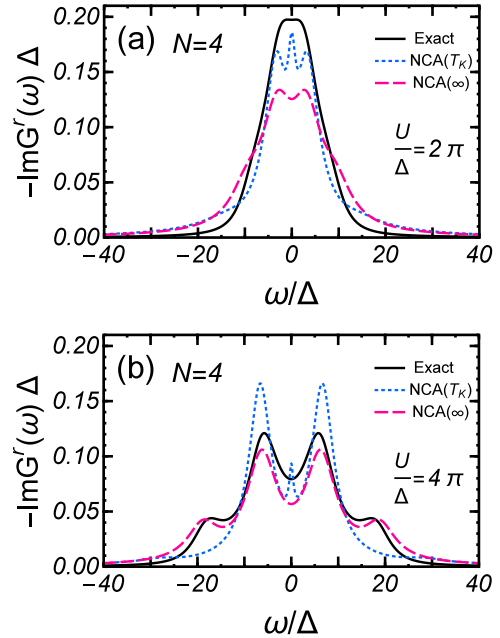

FIG. 5. (Color online) NCA and exact high-temperature results of the equilibrium spectral functions in the SU(4) case for finite interactions, (a) $U/(\pi \Delta) = 2.0$ and (b) 4.0, in the particle-hole-symmetric case $\varepsilon_d = -3U/2$. The solid line denotes the exact $T \to \infty$ results from Eq. (95). The NCA results are obtained (dotted line) numerically at $T = T_K$, and (dashed line) analytically at $T \to \infty$ from Eq. (106). The Kondo temperature is defined by $T_K = \pi z \Delta/4$, with z the renormalization factor deduced from the NRG: (a) $z = 0.52$ for $U = 2.0\pi \Delta$ and (b) $z = 0.25$ for $U = 4.0\pi \Delta$.

the spectral weight at low frequencies $|\omega|/\Delta \lesssim 6.0$, which results in an excess accumulation of the spectral weight in the high-frequency region $|\omega|/\Delta \gtrsim 18.0$ outside the higher-energy peaks. Nevertheless, for $U \gg \Delta$ as in the case of Fig. 5(b), the NCA reasonably describes how the spectral structures evolve at $T \gtrsim T_K$. At $T = T_K$ (dotted line), the Kondo peak is seen at $\omega = 0$ with the two side peaks at $\omega = \pm U/2$ while the other higher-energy peaks still do not appear at $\omega = \pm 3U/2$ and the spectral weight spreads as a wide shoulder at high frequencies $|\omega| \gtrsim 3U/2$. The higher-energy peaks evolve at high temperatures $T \gtrsim U$, and the NCA captures typical features of these changes. Similar features can also be seen in Fig. 5(a) for a weak interaction. However, the NCA becomes less accurate for $U \lesssim \Delta$, where the effects of the hybridizations dominate and the peak structures are smeared.

VIII. SUMMARY

We have described exact high bias properties of the multiorbital Anderson impurity connected to two noninteracting leads. In the limit of $eV \to \infty$, the distribution function $f_{\text{eff}}^{(m)}(\omega)$ becomes a constant independent of ω, and the excitations of whole energy scales equally contribute to the dynamics [25]. Because of this highly symmetric structure of the excitation processes, the time evolution along the Keldysh contour, in the high bias limit, can be described by the effective Lagrangian of a Markovian form [Eqs. (14) and (15)], which has no long-time tail.

We have constructed the corresponding Hamiltonian formulation using the non-Hermitian time-evolution generator $\widehat{H}_{\text{eff}}$. This Hamiltonian is defined with respect to the doubled Hilbert space, which consists of the original Fock space for the real particles and the counterpart for the fictitious particles that represent the time-reversed states along the backward Keldysh contour. The real and fictitious particles satisfy the *boundary* condition in time, given in Eq. (45), at the turnaround point $t \to \infty$ of the Keldysh contour. This ensures the linear dependence of the four components of the nonequilibrium Green's function. The effective Hamiltonian $\widehat{H}_{\text{eff}}$ has a highly symmetrical algebraic structure [Eq. (28)], which can be clearly seen in the expression in terms of the generalized charge and current defined with respect to the enlarged Hilbert space. This represents the essential symmetries that the excitations acquired in the high bias limit.

We have obtained the analytic expression (88) of the Green's function, which is asymptotically exact in the $eV \to \infty$ limit. It shows that many-body effects on the Green's function $G_m^r(t)$ can be factorized in the time representation. This result holds for general orbital-dependent parameters; $\xi_{d,m}$, $\Gamma_{R,m}$, $\Gamma_{L,m}$, and $U_{m'm}$. Furthermore, the continued-fraction representation of $G_m^r(\omega)$ has been obtained for m-independent interactions and hybridizations. The explicit continued-fraction representation, given in Eq. (95), shows that the imaginary part emerges recursively through the relaxation of intermediate states with an incident particle accompanied by excited k particle-hole pairs ($k = 1,2,\ldots,N-1$), which give the damping rate of $(2k-1)\Delta$.

The corresponding spectral function has N separate peaks at $\omega - \xi_{d,m} = -(N-1)U/2,\ldots(N-1)U/2$ for symmetric coupling $\Gamma_L = \Gamma_R$ with strong interactions $U \gg \Delta$. The

coupling asymmetry $\Gamma_L \neq \Gamma_R$ varies the average impurity occupation, and shifts the spectral weight towards high-energy region. We have also examined the temperature dependence of the spectral weight using the NCA, which can be analytically solved for $T \to \infty$. The results demonstrate a typical feature: among the N separate peaks seen in the limit of $T \to \infty$, the ones corresponding to the highest-energy excitations disappear as temperature decreases, and for large N the next-highest ones will also disappear as T decreases further. Our results can also be used as a standard to check theoretical approaches to out-of-equilibrium quantum impurities at high bias voltages.

APPENDIX A: FEYNMAN RULE FOR THE HARTREE TERM

There is a slight difference between the Feynman rules for the Keldysh Green's function $G_m^{\mu\nu}$ and those for the Green's function $\mathcal{G}_m^{\mu\nu}$ defined with respect to the doubled Hilbert space.

It emerges for the $+$ component of the Hartree-type self-energy Σ_m^{++}, which corresponds to the tadpole diagram shown in Fig. 6. As the arguments t and t' for the inner Green's function along the loop are equal, the limit is required to be taken carefully such that $G_m^{++}(t + 0^+, t)$ in the Keldysh approach whereas the opposite limit is required for $\mathcal{G}_m^{++}(t, t + 0^+)$ in the thermal-field-theoretical approach. This is caused by the difference in the direction of the time ordering for the operators belonging to the $+$ branch. Thus, for the $-$ component of the Hartree-type self-energy Σ_m^{--}, the same limit $t' \to t + 0^+$ is taken for both the Keldysh and the thermal-field-theoretical Green's functions.

The effective Hamiltonian $\widehat{H}_{\text{eff}}$, defined in Eqs. (16) and (17), includes the U-dependent terms such that

$$\frac{1}{2}\sum_{m\neq m'}U_{mm'}\,Q_m + \widehat{H}_{\text{eff}}^{(U)}$$
$$= \frac{1}{2}\sum_{m\neq m'}U_{mm'}(n_{-,m}\,n_{-,m'} - n_{+,m}\,n_{+,m'}) + \widehat{H}_{\text{eff}}^{(\text{CT})}. \quad \text{(A1)}$$

The last term includes only the number operators for the $+$ branch,

$$\widehat{H}_{\text{eff}}^{(\text{CT})} \equiv \sum_{m=1}^{N}\sum_{m'(\neq m)}U_{mm'}\left(n_{+,m} - \frac{1}{2}\right), \quad \text{(A2)}$$

and can be regarded a counter term for the particles in the $+$ branch. This term compensates the difference that arises in the $+$ component of the Hartree energy shift, mentioned above.
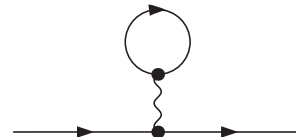

FIG. 6. Feynman diagram for the Hartree term.

APPENDIX B: ATOMIC LIMIT IN THERMAL EQUILIBRIUM

The atomic-limit Green's function in equilibrium takes the following form at finite temperatures:

$$G_m^{(\mathrm{ATM})}(\omega) = \sum_{\mathcal{Q}=0}^{N-1} \binom{N-1}{\mathcal{Q}} \frac{1}{\Xi} \frac{e^{-\beta E_{\mathcal{Q}+1}} + e^{-\beta E_{\mathcal{Q}}}}{\omega - (E_{\mathcal{Q}+1} - E_{\mathcal{Q}})} , \quad \text{(B1)}$$

$$\Xi = \sum_{\mathcal{Q}=0}^{N} \binom{N}{\mathcal{Q}} e^{-\beta E_{\mathcal{Q}}}, \quad E_{\mathcal{Q}} = \mathcal{Q}\,\varepsilon_d + \frac{U}{2}\,\mathcal{Q}(\mathcal{Q}-1) \quad \text{(B2)}$$

in the SU(N) case where quantized level ε_d has N-fold degeneracy [48]. This function has the poles at $\omega = \varepsilon_d + \mathcal{Q}U$ for ω for $\mathcal{Q} = 0, 1, 2, \ldots, N-1$. Equation (B1) coincides with Eq. (104) in the $T \to \infty$ limit.

APPENDIX C: NONCROSSING APPROXIMATION

The closed system of equations of the NCA can be analytically solved in the high-temperature limit $T \to \infty$ at equilibrium $eV = 0$, to yield the expression, given in Eq. (106). In this appendix, we provide the outline of derivation.

1. Basic equations of the NCA

The NCA is a self-consistent perturbation theory, which collects a specific series of expansions in the hybridization [18–21]. This method is known to give physically reasonable result at energy scales near the Kondo temperature. To work in this approximation, we rewrite the Hamiltonian, given by Eqs. (1) and (2), in the form

$$\mathcal{H} = \mathcal{H}_{\mathrm{band}} + \mathcal{H}_{\mathrm{dot}} + \mathcal{H}_{\mathrm{hyb}}, \quad \text{(C1)}$$

$$\mathcal{H}_{\mathrm{band}} = \sum_{m=1}^{N} \int_{-D}^{D} d\epsilon\, \epsilon\, c_{\epsilon m}^{\dagger} c_{\epsilon m}, \quad \text{(C2)}$$

$$\mathcal{H}_{\mathrm{dot}} = \sum_{n=1}^{2^N} E_n \,|n\rangle\langle n|, \quad \text{(C3)}$$

$$\mathcal{H}_{\mathrm{hyb}} = \sum_{m=1}^{N} \sum_{n,n'}^{2^N} \left(v_m M_{n,n'}^m |n\rangle\langle n'|\psi_m + \mathrm{H.c.} \right). \quad \text{(C4)}$$

Here, E_n and $|n\rangle$ are the 2^N many-body eigenvalues and corresponding eigenstates of $\mathcal{H}_{\mathrm{dot}}$ that include the interactions between electrons in the dot. The matrix element $M_{n,n'}^m \equiv \langle n|d_m^{\dagger}|n'\rangle$ is defined between these many-body eigenstates. Note that we consider an equilibrium situation, and therefore only a linear combination of the the conduction bands which couples to the dot $\psi_m \equiv (v_{L,m}\psi_{L,m} + v_{R,m}\psi_{R,m})/v_m$ with $v_m = \sqrt{v_{R,m}^2 + v_{L,m}^2}$ are explicitly shown in the above Hamiltonian.

The NCA for finite interactions can be described by the coupled equations for the retarded resolvents and the self-energies

$$R_n(\omega) = \frac{1}{\omega - E_n - \Sigma_n^{(\mathrm{NCA})}(\omega)}, \quad \text{(C5)}$$

$$\Sigma_n^{(\mathrm{NCA})}(\omega) = \sum_{n'=1}^{2^N} \sum_{m=1}^{N} \frac{\Delta_m}{\pi} \left[\left(M_{n,n'}^m\right)^2 + \left(M_{n',n}^m\right)^2 \right]$$
$$\times \int_{-D}^{D} d\epsilon\, R_{n'}(\omega + \epsilon) f(\epsilon). \quad \text{(C6)}$$

The local density of states at the dot site is given by

$$\rho_{dm}(\omega) = -\frac{1}{\pi}\mathrm{Im}\, G_m^r(\omega)$$

$$= \frac{1}{Z_{\mathrm{total}}/Z_{\mathrm{band}}} \sum_{n,n'}^{2^N} \left(M_{n,n'}^m\right)^2 \int_{-D}^{D} d\epsilon\, e^{-\beta\epsilon}$$

$$\times [\rho_n(\epsilon)\rho_{n'}(\epsilon + \omega) + \rho_n(\epsilon)\rho_{n'}(\epsilon - \omega)], \quad \text{(C7)}$$

with a partition function

$$\frac{Z_{\mathrm{total}}}{Z_{\mathrm{band}}} = \sum_{n=1}^{2^N} \int_{-D}^{D} d\epsilon\, e^{-\beta\epsilon}\, \rho_n(\epsilon), \quad \text{(C8)}$$

and the spectral function for the resolvent

$$\rho_n(\omega) = -\frac{1}{\pi}\,\mathrm{Im}\, R_n(\omega). \quad \text{(C9)}$$

2. High-temperature limit

In the high-temperature limit, the Fermi distribution function in Eq. (C6) is replaced by a constant $\frac{1}{2}$, and the integration can be readily executed to give an ω-independent constant. Then, the NCA equation can be solved and the resolvent is given by a Breit-Wigner form

$$R_n(\omega) = \frac{1}{\omega - E_n + i\Gamma_n}, \quad \text{(C10)}$$

with

$$\Gamma_n = \sum_{n'}^{2^N} \sum_{m}^{N} \frac{\Delta_m}{2}\left[\left(M_{n,n'}^m\right)^2 + \left(M_{n',n}^m\right)^2\right]. \quad \text{(C11)}$$

Substituting these forms into Eq. (C7), the asymptotic form of the local density of state in the limit of $T \to \infty$ can be expressed in a sum of the Lorentzian peaks

$$\rho_{dm}(\omega) = \frac{1}{2^{N-1}} \sum_{n,n'}^{2^N} \left(M_{n,n'}^m\right)^2 \frac{\Gamma_n + \Gamma_{n'}}{\pi}$$

$$\times \frac{1}{[\omega - (E_{n'} - E_n)]^2 + (\Gamma_n + \Gamma_{n'})^2}. \quad \text{(C12)}$$

Particularly, for the m-independent interactions and hybridizations $U_{mm'} \equiv U$ and $\Delta_m \equiv \Delta$, the asymptotic expressions can be more simplified because Γ_n in this case is explicitly in the form

$$\Gamma_n = \frac{N\Delta}{2}. \quad \text{(C13)}$$

Then, Eq. (C12) corresponds to the NCA Green's function given in Eq. (106).

[1] A. C. Hewson, *The Kondo Problem to Heavy Fermions* (Cambridge University Press, Cambridge, 1993).

[2] A. Yoshimori, Prog. Theor. Phys. **55**, 67 (1976).

[3] M. Grobis, I. G. Rau, R. M. Potok, H. Shtrikman, and D. Goldhaber-Gordon, Phys. Rev. Lett. **100**, 246601 (2008).

[4] G. D. Scott, Z. K. Keane, J. W. Ciszek, J. M. Tour, and D. Natelson, Phys. Rev. B **79**, 165413 (2009).

[5] O. Zarchin, M. Zaffalon, M. Heiblum, D. Mahalu, and V. Umansky, Phys. Rev. B **77**, 241303 (2008).

[6] Y. Yamauchi, K. Sekiguchi, K. Chida, T. Arakawa, S. Nakamura, K. Kobayashi, T. Ono, T. Fujii, and R. Sakano, Phys. Rev. Lett. **106**, 176601 (2011).

[7] T. Delattre, C. Feuillet-Palma, L. G. Herrmann, P. Morfin, J.-M. Berroir, G. Fève, B. Plaçais, D. C. Glattli, M.-S. Choi, C. Mora, and T. Kontos, Nat. Phys. **5**, 208 (2009).

[8] J. Basset, A. Yu. Kasumov, C. P. Moca, G. Zaránd, P. Simon, H. Bouchiat, and R. Deblock, Phys. Rev. Lett. **108**, 046802 (2012).

[9] C. Mora, P. Vitushinsky, X. Leyronas, A. A. Clerk, and K. Le Hur, Phys. Rev. B **80**, 155322 (2009).

[10] R. Sakano, T. Fujii, and A. Oguri, Phys. Rev. B **83**, 075440 (2011).

[11] R. Sakano, A. Oguri, T. Kato, and S. Tarucha, Phys. Rev. B **83**, 241301 (2011).

[12] R. Sakano, Y. Nishikawa, A. Oguri, A. C. Hewson, and S. Tarucha, Phys. Rev. Lett. **108**, 266401 (2012).

[13] F. B. Anders, Phys. Rev. Lett. **101**, 066804 (2008).

[14] S. Kirino, T. Fujii, J. Zhao, and K. Ueda, J. Phys. Soc. Jpn. **77**, 084704 (2008).

[15] P. Werner, T. Oka, and A. J. Millis, Phys. Rev. B **79**, 035320 (2009).

[16] L. Mühlbacher, D. F. Urban, and A. Komnik, Phys. Rev. B **83**, 075107 (2011).

[17] J. E. Han, A. Dirks, and T. Pruschke, Phys. Rev. B **86**, 155130 (2012).

[18] N. Bickers, Rev. Mod. Phys. **59**, 845 (1987).

[19] H. Keiter and Q. Qin, Physica B (Amsterdam) **163**, 594 (1990).

[20] J. Kroha and P. Wölfle, J. Phys. Soc. Jpn. **74**, 16 (2005).

[21] J. Otsuki and Y. Kuramoto, J. Phys. Soc. Jpn. **75**, 064707 (2006).

[22] N. S. Wingreen and Y. Meir, Phys. Rev. B **49**, 11040 (1994).

[23] A. Oguri, R. Sakano, and T. Fujii, Phys. Rev. B **84**, 113301 (2011).

[24] A. Oguri, Phys. Rev. B **85**, 155404 (2012).

[25] A. Oguri, J. Phys. Soc. Jpn. **71**, 2969 (2002).

[26] A. Oguri and R. Sakano, Phys. Rev. B **88**, 155424 (2013).

[27] S. Hershfield, J. H. Davies, and J. W. Wilkins, Phys. Rev. B **46**, 7046 (1992).

[28] Y. Meir and N. S. Wingreen, Phys. Rev. Lett. **68**, 2512 (1992).

[29] A. Kaminski, Yu. V. Nazarov, and L. I. Glazman, Phys. Rev. B **62**, 8154 (2000).

[30] A. Oguri, Phys. Rev. B **64**, 153305 (2001).

[31] A. C. Hewson, J. Bauer, and A. Oguri, J. Phys.: Condens. Matter **17**, 5413 (2005).

[32] A. O. Gogolin and A. Komnik, Phys. Rev. B **73**, 195301 (2006).

[33] E. Sela, Y. Oreg, F. von Oppen, and J. Koch, Phys. Rev. Lett. **97**, 086601 (2006)

[34] A. Golub, Phys. Rev. B **73**, 233310 (2006).

[35] T. Fujii, J. Phys. Soc. Jpn. **79**, 044714 (2010).

[36] L. V. Keldysh, Zh. Eksp. Teor. Fiz. **47**, 1515 (1964) [Sov. Phys.– JETP **20**, 1018 (1965)].

[37] C. Caroli, R. Combescot, P. Nozieres, and D. Saint-James, J. Phys. C: Solid State Phys. **4**, 916 (1971).

[38] H. Umezawa, H. Matsumoto, and M. Tachiki, *Thermo Field Dynamics and Condensed States* (North-Holland, Amsterdam, 1982).

[39] H. Ezawa, T. Arimitsu, and Y. Hashimoto, *Thermal Field Theories* (North-Holland, Amsterdam, 1991).

[40] J. Hubbard, Proc. R. Soc. A**276**, 238 (1963).

[41] S. Doniach, Adv. Phys. **18**, 819 (1969).

[42] H. Haug and A.-P. Jauho, *Quantum Kinetics in Transport and Optics of Semiconductors* (Springer, Berlin, 1996).

[43] M. Esposito, U. Harbola, and S. Mukamel, Rev. Mod. Phys. **81**, 1665 (2009).

[44] A. A. Dzhioev and D. S. Kosov, J. Chem. Phys. **134**, 154107 (2011).

[45] R. B. Saptsov and M. R. Wegewijs, Phys. Rev. B **86**, 235432 (2012).

[46] R. B. Saptsov and M. R. Wegewijs, Phys. Rev. B **90**, 045407 (2014).

[47] We are using a standard notation of the thermal field theory and the Liouville-Fock space approach for the initial and final states, i.e., $\langle\!\langle I \|$ and $\| \rho \rangle\!\rangle$ [39,43]. With these approaches, a mixed-state average defined in the original Hilbert space can be reformulated as a pure-state average with respect to these two states in the enlarged Hilbert space. The statistical density weight can be described through $\| \rho \rangle\!\rangle$ while $\langle\!\langle I \|$ plays a role of the projection operator onto the physical subspace.

[48] J. Hubbard, Proc. R. Soc. A**277**, 237 (1964).